PROCEEDINGS OF SCIENCE

Scattering from generalised lattice ϕ^4 theory

Marco Garofalo ,[a,*] **Fernando Romero-López,**[b,c] **Akaki Rusetsky**[a,d] **and Carsten Urbach**[a]

[a] *HISKP (Theory), Rheinische Friedrich-Wilhelms-Universität Bonn, Nussallee 14-16, 53115 Bonn, Germany*

[b] *Center for Theoretical Physics, Massachusetts Institute of Technology,Cambridge, MA 02139, USA*

[c] *IFIC, CSIC-Universitat de València, 46980 Paterna, Spain*

[d] *Tbilisi State University, 0186 Tbilisi, Georgia*

E-mail: garofalo@hiskp.uni-bonn.de

We investigate numerically different techniques to extract scattering amplitudes from the Euclidean Lattice ϕ^4 theory with two fields, having different masses. We present an exploratory study of the recently proposed method by Bruno and Hansen for extracting the scattering length from a four-point function [1], and a study of the two- and three-particle quantization condition.

The 38th International Symposium on Lattice Field Theory, LATTICE2021 26th-30th July, 2021
Zoom/Gather@Massachusetts Institute of Technology
Report number: MIT-CTP/5366

*Speaker

PoS(LATTICE2021)384

1. Introduction

The standard approach to determine scattering quantities from Lattice QCD is the Lüscher method [2], which relates the finite-volume spectrum obtained from the lattice to the infinite-volume scattering amplitude. It has been applied to many physical systems, see Ref. [3] for a review. The formalism has also been recently extended to three particles with three different but conceptually equivalent formulations available in the literature at present [4–8], see Refs. [9, 10] for recent reviews.

In this contribution we study the techniques to extract scattering amplitudes from the Euclidean Lattice field theory. We use a Euclidean Lattice ϕ^4 theory with two fields having different masses. Using this theory has proven to be an excellent test environment for novel scattering studies, as shown in Refs. [11–13].

In particular we study the recent proposal [1], in which the authors found a relation between the scattering length and the Euclidean four-point functions at threshold kinematic. Henceforth, this will be referred to as the BH method. We compare the BH method to the standard Lüscher approach and find good agreement. This study of the BH method presented here is based on [14].

We also investigate the extraction of the scattering quantities at non-zero momentum. In particular we studied s-wave scattering amplitude for two particles with the Lüscher method [15].

2. Description of the Model

The Euclidean model used here is composed of two real scalar fields $\phi_i, i = 0, 1$ with the Lagrangian

$$\mathcal{L} = \sum_{i=0,1} \left(\frac{1}{2} \partial_\mu \phi_i \partial_\mu \phi_i + \frac{1}{2} m_i \phi_i^2 + \lambda_i \phi_i^4 \right) + \mu \phi_0^2 \phi_1^2 , \tag{1}$$

with nondegenerate (bare) masses $m_0 < m_1$. The Lagrangian has a $Z_2 \otimes Z_2$ symmetry $\phi_0 \to -\phi_0$ and $\phi_1 \to -\phi_1$, which prevents sectors with even and odd number of particles to mix.

To study the problem numerically, we define the theory on a finite hypercubic lattice with lattice spacing a and a volume $T \cdot L^3$, where T denotes the Euclidean time length and L the spatial length. We define the derivatives of the Lagrangian (1) on a finite lattice as the finite differences $\partial_\mu \phi(x) = \frac{1}{a} (\phi(x + a\mu) - \phi(x))$. In addition, periodic boundary conditions are assumed in all directions. The discrete action is given in Ref. [12] for the complex scalar theory, but it is trivial to adapt it to this case. We set $a = 1$ in the following for convenience.

3. The BH method

In Ref. [1], Bruno and Hansen derived a relation between the scattering length a_0 and the following combination of Euclidean four-point and two-point correlation functions at the two-particle threshold:

$$C_4^{\mathrm{BH}}(t_f, t, t_i) \equiv \frac{\langle \tilde{\phi}_0(t_f, 0) \tilde{\phi}_1(t, 0) \tilde{\phi}_1(t_i, 0) \tilde{\phi}_0(0, 0) \rangle}{\langle \tilde{\phi}_0(t_f, 0) \tilde{\phi}_0(0, 0) \rangle \langle \tilde{\phi}_1(t, 0) \tilde{\phi}_1(t_i, 0) \rangle} - 1, \tag{2}$$

with the time ordering $t_f > t > t_i > 0$, and $\tilde{\phi}_i(t,\mathbf{p}) = \sum_{\mathbf{x}} e^{i\mathbf{p}\cdot\mathbf{x}}\phi_i(t,\mathbf{x})$ being spatial Fourier transform of the field. In particular $\tilde{\phi}_i(t,0)$ is the field projected to zero spatial momentum. The relation of C_4^{BH} to the scattering length reads

$$C_4^{\mathrm{BH}}(t_f,t,t_i) \xrightarrow[t\gg t_i\gg 0]{T\gg t_f\gg t} \frac{2}{L^3}\left[\pi\frac{a_0}{\mu_{01}}(t-t_i) - 2a_0^2\sqrt{\frac{2(t-t_i)}{\mu_{01}}} + O\left((t-t_i)^0\right)\right], \tag{3}$$

where $\mu_{01} = (M_0M_1)/(M_0+M_1)$ is the reduced mass. It is defined in terms of the renormalized masses M_0 and M_1 of the two particles. These masses can be extracted as usual from an exponential fit at large time distances of the two-point correlation functions

$$\langle\tilde{\phi}_i(t,\mathbf{p})\tilde{\phi}_i(0,-\mathbf{p})\rangle \approx A_{1,i}\left(e^{-E_1^i(\mathbf{p})t} + e^{-E_1^i(\mathbf{p})(T-t)}\right) \tag{4}$$

with $E_1^i(\mathbf{p}=0) = M_i$ for $i = 0, 1$. To reduce the statistical error we average over all points with the same source sink separation.

3.1 Numerical result

We generate ensembles using the Metropolis-Hastings algorithm with the bare masses $m_0 = -4.925$ and $m_1 = -4.85$, and for simplicity we choose $\lambda_0 = \lambda_1 = 2\mu = 2.5$. The list of ensembles generated in this work with their corresponding measured values of the masses M_0 and M_1 are compiled in table 1. In this model, two-point correlators are dominated by the ground state from the first time slice. This was also observed in previous investigations of the scalar theory [13].

We tried three different strategies to extract the scattering length:

1. We attempt a direct fit of eq. (3) the the data.
2. We include an overall constant in the fit to account for the $O\left((t-t_i)^0\right)$ effect.
3. We make use of the shifted function at fixed t_i and t_f, $\Delta_t C_4^{\mathrm{BH}}(t_f,t,t_i) = C_4^{\mathrm{BH}}(t_f,t+1,t_i) - C_4^{\mathrm{BH}}(t_f,t,t_i)$, where the constant term cancels out. We then determine a_0 by fitting to

$$\Delta_t C_4^{\mathrm{BH}}(t_f,t,t_i) \approx \frac{2}{L^3}\left[\pi\frac{a_0}{\mu_{01}} - 2a_0^2\sqrt{\frac{2}{\mu_{01}}}\left(\sqrt{t+1-t_i} - \sqrt{t-t_i}\right)\right]. \tag{5}$$

The three methods are compared in the left panel of fig. 1 for one of our ensembles. The black triangles represent the correlator of eq. (3) with $t_i = 3$ and $t_f = 16$ divided by $(t-t_i)$ so that it goes to a constant when $(t-t_i) \to \infty$. The monotonic increase of the data points could be due to the $\left((t-t_i)^0\right)$ term in eq. (3). A fit to the formula eq. (3) in the time region $[10, 14]$—the black band—gives a good $\chi^2/d.o.f \sim 0.7$, but results in large uncertainties. The quality of the fit deteriorates very quickly if the fit range is extended: a fit in the time region $[6, 14]$ yields $\chi^2/\mathrm{dof} \sim 5$.

With the second strategy—the red band in the left panel of fig. 1—one is able to start fitting at significantly smaller t-values. The data are well described with a $\chi^2/\mathrm{dof} \sim 0.2$

For the third approach, we study $\Delta_t C_4^{\mathrm{BH}}(t)$. This is shown in the left panel of fig. 1 as blue circles, and the blue band represents the best fit result with error. The main advantage of the latter strategy is that it allows us to extract the physical information at smaller t without introducing extra

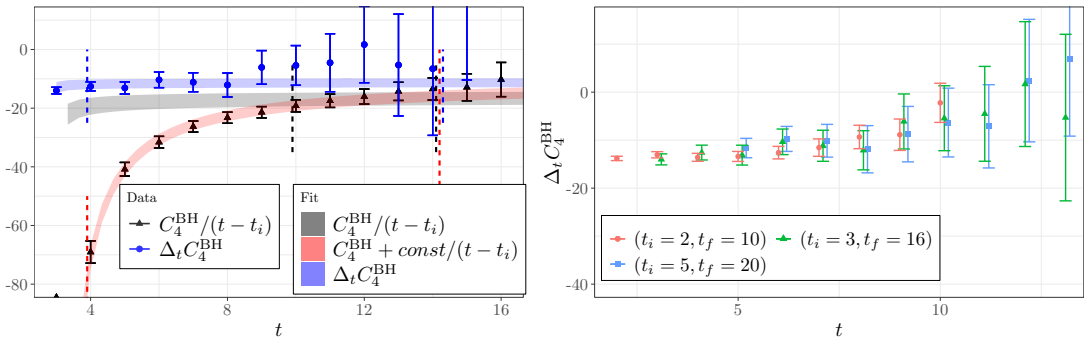

Figure 1: Left panel: Four-point function of eq. (3) multiplied by $L^3/2$, for $L = 22$ and $T = 96$ with $t_i = 3$ and $t_f = 16$ divided by $(t - t_i)$ (black triangles). the dashed vertical lines represent the fit interval, the black band represent the result of the fit eq. (3) and the red band is the same fit with an extra constant term. The blue circles and band represent the discrete derivative of the correlator eq. (5) and the corresponding fit. Right panel: Plot of the discrete derivative of the correlator eq. (5) for different values of t_i and t_f. We do not observe any systematic shift and all correlators are compatible. The points with smaller t_i and t_f tend to have smaller error.

parameters in the fit. Indeed, the data looks almost constant over the complete t-range available. Only very close to t_i the square root term might become visible.

For the third strategy, which looks most promising from a systematic point of view, we also investigate the dependence on the choice of t_i and t_f. This is shown in right panel of fig. 1 for the same ensemble as in the left panel. We do not observe any significant systematic effect stemming from excited state contributions when changing t_i or t_f. However, we clearly see significantly smaller statistical uncertainties with smaller t_i and t_f values.

3.2 Comparison to the Lüscher method

In this section we compare the BH method described above with the Lüscher threshold expansion [16, 17]. The latter relates the two-particle energy shift, defined as $\Delta E_2^{01} = E_2^{01} - M_0 - M_1$, to the scattering length a_0 via

$$\Delta E_2^{01} = -\frac{2\pi a_0}{\mu_{01} L^3}\left[1 + c_1\frac{a_0}{L} + c_2\left(\frac{a_0}{L}\right)^2\right] + O\left(L^{-6}\right), \tag{6}$$

with $c_1 = -2.837297$, $c_2 = 6.375183$ and E_2^{01} being the interacting two-particle energy at zero total momentum. E_2^{01} can be extracted from $C_2(t) = \langle\tilde{\phi}_1(t,0)\tilde{\phi}_0(t,0)\tilde{\phi}_1(0,0)\tilde{\phi}_0(0,0)\rangle$, whose large-$t$ behaviour is

$$C_2(t) \xrightarrow[T-t\gg 0]{t\gg 0} A_2 e^{-E_2^{01}\frac{T}{2}} \cosh\left(E_2^{01}(t-\frac{T}{2})\right) + B_2 e^{-(M_0+M_1)\frac{T}{2}} \cosh\left((M_1-M_0)(t-\frac{T}{2})\right). \tag{7}$$

with the last term being a thermal pollution due to finite T with periodic boundary condition. Using M_0 and M_1 as input determined from the corresponding two-point functions, the only additional parameter is B_2. Alternatively, it is possible to eliminate the second term defining $\tilde{C}_2(t) = C_2(t)/\cosh\left((M_1 - M_0)(t - \frac{T}{2})\right)$, and then taking the finite derivative

$$\Delta_t \tilde{C}_2(t) = \tilde{C}_2(t+1) - \tilde{C}_2(t). \tag{8}$$

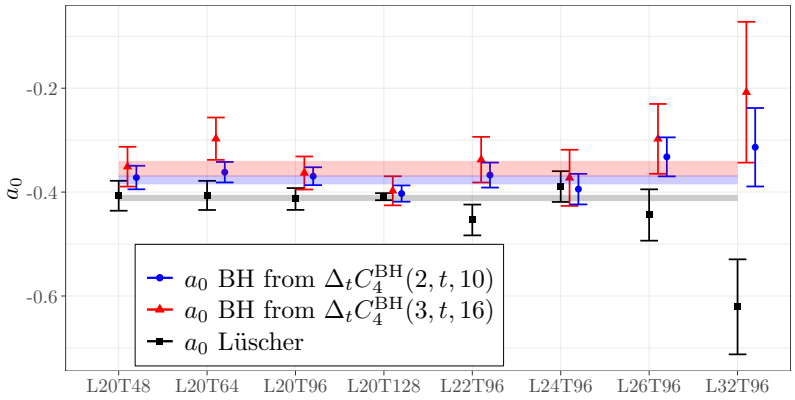

Figure 2: Comparison of a_0 computed with BH method eq. (5) with $t_i = 2$ and $t_f = 10$ (blue circles), with $t_i = 3$ and $t_f = 16$ (red triangles) and Lüscher method eq. (6) (black squares) the horizontal bands correspond to the weighted average of each method.

The two-particle energies obtained from eq. (7) are compatible with those from eq. (8). The results are reported in table 1, along with the values for the scattering length a_0 computed from E_2 using eq. (6). A comparison between the BH and the Lüscher method is depicted in fig. 2 for all our ensembles. The values are compatible with each other. However, the BH method gives systematically larger values for a_0. For each ensemble separately Lüscher and BH methods appear compatible. However we observe a systematic trend after averaging over all ensembles, as shown in the bands of fig. 2. This might be attributed to different lattice artifacts. The statistical error is similar in both approaches. Also, the scaling in L appears to be similar. The different systematics of the two methods offer in general a useful opportunity for cross-checks.

4. Scattering amplitude at not zero momentum with the Lüscher method

In this section, we report our study of the s-wave scattering amplitude for two particles with the Lüscher method [15]. We compute the spectrum of our ϕ^4 model at $\mathbf{p} \neq 0$ for the lighter particle. We generate ensembles using the Metropolis-Hastings algorithm with bare masses $m_0 = -4.9$ and $m_1 = -4.65$, to have $M_1 \sim 3M_0$, keeping $\lambda_0 = \lambda_1 = 2\mu = 2.5$. We extract the energies from an exponential fit to eq. (4) with the discretised momentum $\mathbf{p} = 2\pi\mathbf{n}/L$ with $\mathbf{n}$ being a integer vector in the set $\mathbf{n} \in \{(0,0,0),(1,0,0),(1,1,0),(1,1,1)\}$. As we can see from the left panel of fig. 3, we find that the measured one-particle energies $E_1^0(\mathbf{p})$ significantly deviate from the continuum dispersion relation, while they are in good agreement with the lattice dispersion relation

$$\cosh\left(E_1^0(\mathbf{p})\right) = \cosh(M_0) + \frac{1}{2}\left(\sum_{i=1}^{3} 4\sin\left(\frac{p_i}{2}\right)^2\right), \tag{9}$$

with M_0 being the mass measured in the fitted in eq. (4) at zero momentum.

For each choice of the momentum we construct the two-particle operator in the A1 irrep of the cubic group $\hat{O}_2(t,\mathbf{p}) = \tilde{\phi}_{\mathbf{0}}(\mathbf{t},\mathbf{p})\tilde{\phi}_{\mathbf{0}}(\mathbf{t},\mathbf{0})$. Only for the first unit of momentum we construct the

T	L	M_0	M_1	E_2^{01}		a_0 Lüscher		a_0 BH		
				C_2	$\Delta_t\tilde{C}_2$	C_2	$\Delta_t\tilde{C}_2$	$\Delta_t C_4^{\rm BH}$(3,t,16)	$C_4^{\rm BH}+c$	$\Delta_t C_4^{\rm BH}$(2,t,10)
48	20	0.14675(5)	0.27487(5)	0.4252(3)	0.4253(3)	-0.41(3)	-0.42(3)	-0.35(4)	-0.35(6)	-0.37(2)
64	20	0.14659(5)	0.27480(5)	0.4249(3)	0.4250(3)	-0.41(3)	-0.41(4)	-0.30(4)	-0.29(6)	-0.38(2)
96	20	0.14662(4)	0.27487(4)	0.4251(2)	0.4251(3)	-0.41(2)	-0.41(3)	-0.36(3)	-0.36(4)	-0.38(1)
96	22	0.14604(3)	0.27470(4)	0.4237(2)	0.4237(3)	-0.45(3)	-0.45(5)	-0.34(4)	-0.31(6)	-0.37(2)
96	24	0.14574(4)	0.27458(4)	0.4223(2)	0.4221(3)	-0.39(3)	-0.36(6)	-0.36(5)	-0.41(7)	-0.39(2)
96	26	0.14547(4)	0.27455(3)	0.4218(2)	0.4219(3)	-0.44(5)	-0.47(8)	-0.30(7)	-0.3(1)	-0.36(3)
96	32	0.14521(4)	0.27449(4)	0.4210(2)	0.4213(3)	-0.62(9)	-0.7(1)	-0.2(1)	-0.1(2)	-0.35(5)
128	20	0.14668(3)	0.27484(3)	0.42509(7)	0.4251(3)	-0.409(7)	-0.41(3)	-0.40(3)	-0.39(3)	-0.40(1)

Table 1: Measured values of a_0, M_0, M_1 and E_2. The column $\Delta_t C_4^{\rm BH}$ corresponds to the value of a_0 fitted with eq. (5) fixing $t_i = 3$ and $t_f = 16$ or $t_i = 2$ and $t_f = 10$. The column $C_{\rm BH} + c$ is the result of the fit with eq. (3) adding a constant term. The two-particle energy E_2 is computed from C_2 with the fit of eq. (7) and from $\Delta\tilde{C}_2$ with eq. (8). The corresponding value of a_0 computed with the Lüscher method is reported in the corresponding columns. We used $2 \cdot 10^7$ configurations for each ensemble, generated from 200 replicas each of 10^5 thermalized configurations. We bin the configurations in blocks of 10^5 (the entirely replica) and we resample the resulting 200 configurations with jackknife. For the light mass M_0 we measured the integrated autocorrelation time $\tau_{int} \sim 1.5$, while $\tau_{int} \sim 0.5$ for M_1. We skip 1000 configurations in each replica for thermalization.

operator with back to back momentum still in the A_1 irrep $\hat{O}_2(t,0) = \sum_{i=x,y,z} \tilde{\phi}_0(t,p_i)\tilde{\phi}_0(t,-p_i)$ with $p_x = (2\pi/L, 0, 0)$, $p_y = (0, 2\pi/L, 0)$ and $p_z = (0, 0, 2\pi/L)$. We measured the two-particle energy from the exponential fit of the correlator

$$\langle \hat{O}_2(t,\mathbf{p})\hat{O}_2(0,-\mathbf{p})\rangle \xrightarrow[T-t\gg 0]{t\gg 0} A_2 e^{-E_2^0(\mathbf{p})\frac{T}{2}} \cosh\left(E_2^0(\mathbf{p})(t-\frac{T}{2})\right) \tag{10}$$

$$+A_1 e^{-(E_1^0(\mathbf{p})+M_0)\frac{T}{2}} \cosh\left((E_1^0(\mathbf{p})-M_0)(t-\frac{T}{2})\right), \tag{11}$$

where $E_1^0(\mathbf{p})$ and M_0 are the ones obtained from the fit of eq. (4). From the two-particle energies $E_2^0(\mathbf{p})$ we calculate the s-wave phase shift as [15]

$$\cot\delta = \frac{Z_{0,0}(1,q^2)}{\pi^{3/2}\gamma q}, \tag{12}$$

where $Z_{0,0}$ is the Lüscher zeta function, the Lorentz boost $\gamma = E_2^0(\mathbf{p})/E_{CM}$ is defined in terms of center of mass energy $E_{CM} = E_2^0(\mathbf{p}) - \mathbf{p}^2$ and $q = kL/2\pi$ with the scattering momentum $k = \frac{E_{CM}}{4} - M_0^2$. We notice that, at large momentum $\mathbf{p}$, the values of the phase shift computed with eq. (12) come with large errors (red circles of fig. 3). These large errors stem from the fact that the energies deviate significantly from the continuum dispersion relation. This problem was also observed in [18], where as a solution the author propose to compute the center of mass energy E_{CM} using the lattice dispersion relation. Here we follow a similar strategy. We subtract the difference between the free two -particle energies $E_2^{free,latt} - E_2^{free,cont}$ computed with the lattice eq. (9) and continuum dispersion relation from the two-particle energy. The factor $E_2^{free,latt} - E_2^{free,cont}$ is a lattice artifact, i.e. it goes to zero in the continuum limit. However, at finite lattice spacing, we notice a reduction of the statistical error in the phase shift computed from energies at large momentum fig. 3 (blue point of the right panel of fig. 3).

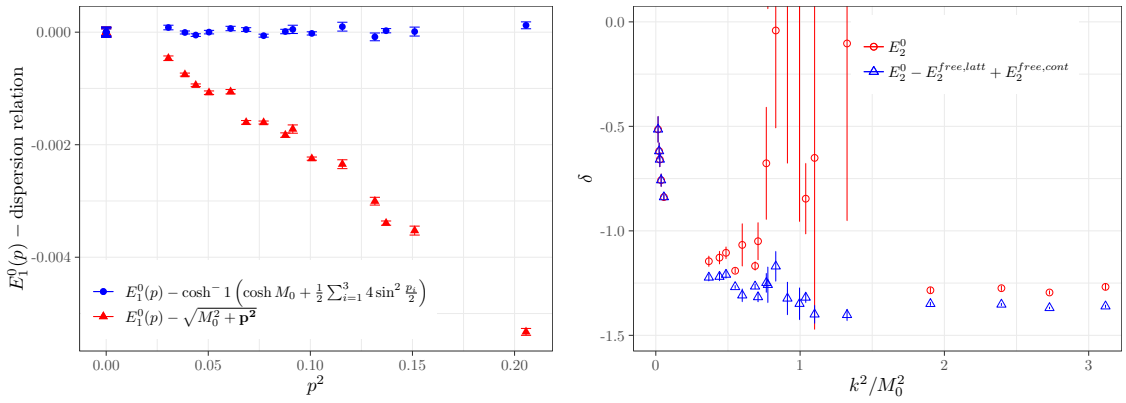

Figure 3: Left panel: Values of the energies level measured for different values of p^2 minus the value predicted using the lattice dispersion relation (blue circles) or the continuum dispersion relation (red triangles). Right panel: values of the phases shift δ obtained from eq. (12) using as input the two-particle energies measured on the lattice (red circles) or the energies corrected by a lattice artifact $E_2^{free,latt} - E_2^{free,cont}$ (blue point). The statistic used is the same as described in the caption of table 1.

5. Conclusion

In this contribution, we studied the BH method, proposed in [1]. We have verified that it produces results that are compatible with those of the Lüscher method [16]. We also studied the s-wave scattering amplitude for two particles with the Lüscher method at non-zero momentum [15]. As in [18], we observed that the error on the computed phase shift becomes larger with the momentum of the two-particle state. This increase of the error can be mitigated by the subtraction of a lattice artifact in the measured energy.

6. Acknowledgements

We gratefully acknowledge helpful discussions with M. Bruno, M. T. Hansen and S. R. Sharpe. FRL acknowledges financial support from Generalitat Valenciana grants PROMETEO/2019/083 and CIDEGENT/2019/040, the EU project H2020-MSCA-ITN-2019//860881-HIDDeN, and the Spanish project FPA2017-85985-P. The work of FRL is supported in part by the U.S. Department of Energy, Office of Science, Office of Nuclear Physics, under grant Contract Numbers DE-SC0011090 and DE-SC0021006. This work is supported in part by the Deutsche Forschungsgemeinschaft (DFG, German Research Foundation) and the NSFC through the funds provided to the Sino-German Collaborative Research Center CRC 110 “Symmetries and the Emergence of Structure in QCD” (DFG Project-ID 196253076 - TRR 110, NSFC Grant No. 12070131001). AR acknowledges support from Volkswagenstiftung (Grant No. 93562) and the Chinese Academy of Sciences (CAS) President’s International Fellowship Initiative (PIFI) (Grant No. 2021VMB0007). The C++ Performance Portability Programming Model Kokkos [19] and the open source software packages R [20] have been used. We thank B. Kostrzewa for useful discussions on Kokkos.

References

[1] Mattia Bruno and Maxwell T. Hansen. Variations on the Maiani-Testa approach and the inverse problem. *Journal of High Energy Physics*, 2021(6), Jun 2021.

[2] Martin Lüscher and Ulli Wolff. How to Calculate the Elastic Scattering Matrix in Two-dimensional Quantum Field Theories by Numerical Simulation. *Nucl. Phys.*, B339:222–252, 1990.

[3] Raul A. Briceno, Jozef J. Dudek, and Ross D. Young. Scattering processes and resonances from lattice QCD. *Rev. Mod. Phys.*, 90(2):025001, 2018.

[4] Maxwell T. Hansen and Stephen R. Sharpe. Relativistic, model-independent, three-particle quantization condition. *Phys. Rev. D*, 90(11):116003, 2014.

[5] Maxwell T. Hansen and Stephen R. Sharpe. Expressing the three-particle finite-volume spectrum in terms of the three-to-three scattering amplitude. *Phys. Rev. D*, 92(11):114509, 2015.

[6] Hans-Werner Hammer, Jin-Yi Pang, and A. Rusetsky. Three-particle quantization condition in a finite volume: 1. The role of the three-particle force. *JHEP*, 09:109, 2017.

[7] H. W. Hammer, J. Y. Pang, and A. Rusetsky. Three particle quantization condition in a finite volume: 2. general formalism and the analysis of data. *JHEP*, 10:115, 2017.

[8] M. Mai and M. Döring. Three-body Unitarity in the Finite Volume. *Eur. Phys. J. A*, 53(12):240, 2017.

[9] Maxwell T. Hansen and Stephen R. Sharpe. Lattice QCD and Three-particle Decays of Resonances. *Ann. Rev. Nucl. Part. Sci.*, 69:65–107, 2019.

[10] Maxim Mai, Michael Döring, and Akaki Rusetsky. Multi-particle systems on the lattice and chiral extrapolations: a brief review. *EPJ ST*, 06 2021.

[11] Stephen R. Sharpe. Testing the threshold expansion for three-particle energies at fourth order in ϕ^4 theory. *Phys. Rev. D*, 96(5):054515, 2017. [Erratum: Phys.Rev.D 98, 099901 (2018)].

[12] Fernando Romero-López, Akaki Rusetsky, and Carsten Urbach. Two- and three-body interactions in φ^4 theory from lattice simulations. *Eur. Phys. J. C*, 78(10):846, 2018.

[13] Fernando Romero-López, Akaki Rusetsky, Nikolas Schlage, and Carsten Urbach. Relativistic N-particle energy shift in finite volume. *JHEP*, 02:060, 2021.

[14] Marco Garofalo, Fernando Romero-López, Akaki Rusetsky, and Carsten Urbach. Testing a new method for scattering in finite volume in the ϕ^4 theory. 7 2021.

[15] Martin Lüscher. Two-particle states on a torus and their relation to the scattering matrix. *Nuclear Physics B*, 354(2):531–578, 1991.

[16] M. Lüscher. Volume Dependence of the Energy Spectrum in Massive Quantum Field Theories. 1. Stable Particle States. *Commun.Math.Phys.*, 104:177, 1986.

[17] S.R. Beane, P.F. Bedaque, A. Parreño, and M.J. Savage. A framework for exploring the interactions and decays of hyperons with lattice qcd. *Nuclear Physics A*, 747(1):55–74, Jan 2005.

[18] K. Rummukainen and Steven Gottlieb. Resonance scattering phase shifts on a non-rest-frame lattice. *Nuclear Physics B*, 450(1):397–436, 1995.

[19] Christian R. Trott et al. Kokkos 3: Programming model extensions for the exascale era. *IEEE Transactions on Parallel and Distributed Systems*, 33(4):805–817, 2022.

[20] R Core Team. *R: A Language and Environment for Statistical Computing*. R Foundation for Statistical Computing, Vienna, Austria, 2019.